Resident and recruited macrophages differentially contribute to cardiac healing after myocardial ischemia

Tobias Weinberger[1,2,3,4], Denise Messerer[1,2], Markus Joppich[5], Max Fischer[1,2,3], Clarisabel Garcia[4], Konda Kumaraswami [1,2], Vanessa Wimmler[1,2], Sonja Ablinger[1,2], Saskia Räuber[1,2,6], Jiahui Fang[1,2], Lulu Liu[1,2], Wing Han Liu[1], Julia Winterhalter[1,2], Johannes Lichti[1], Lukas Tomas[1,2,3], Dena Esfandyari[3,7], Guelce Percin[8], Sandra Martin Salamanca[9], Andres Hidalgo[9,10], Claudia Waskow[8,11], Stefan Engelhardt[3,7], Andrei Todica[12], Ralf Zimmer[5], Clare Pridans[13,14], Elisa Gomez-Perdiguero[4], Christian Schulz[1,2,3]

[1]Medical Clinic I., Department of Cardiology, University Hospital, Ludwig Maximilian University, 81377 Munich, Germany

[2]Institute of Surgical Research at the Walter-Brendel-Centre of Experimental Medicine, University Hospital, Ludwig Maximilian University, 81377 Munich, Germany

[3]DZHK (German Centre for Cardiovascular Research), partner site Munich Heart Alliance, 80336 Munich, Germany

[4]Institut Pasteur, Unité Macrophages et Développement de l'Immunité, Département de Biologie du Développement et Cellules Souches, Paris, France

[5]LFE Bioinformatik, Department of Informatics, Ludwig Maximilian University, 80333 Munich, Germany

[6]Department of Neurology, Medical Faculty, Heinrich Heine University of Düsseldorf, 40225 Düsseldorf, Germany

[7]Institute of Pharmacology and Toxicology, Technical University Munich, 80802 Munich, Germany

[8]Immunology of Aging, Leibniz-Institute on Aging - Fritz-Lipmann-Institute (FLI), 07745 Jena, Germany

[9]Area of Cell & Developmental Biology, Centro Nacional de Investigaciones Cardiovasculares Carlos III, Madrid, Spain

[10]Vascular Biology and Therapeutics Program and Department of Immunobiology, Yale University School of Medicine, New Haven, CT, USA

[11]Faculty of Biological Sciences, Friedrich-Schiller-University, 07737 Jena, Germany

[12]Department of Nuclear Medicine, Ludwig Maximilian University, 81377 Munich, Germany

[13]University of Edinburgh Centre for Inflammation Research, The Queen's Medical Research Institute, Edinburgh EH16 4TJ, United Kingdom.

[14]Simons Initiative for the Developing Brain, Centre for Discovery Brain Sciences, University of Edinburgh, Edinburgh EH8 9XD, United Kingdom

Corresponding author: Dr. Christian Schulz, MD

Address: Medical Clinic I., Department of Cardiology, University Hospital, Ludwig Maximilian University, Marchioninistrasse 15, 81377 Munich, Germany

Phone: +49 89 440073092

Email: Christian.schulz@med.un-muenchen.de

Conflict-of-interest statement: The authors have declared that no conflict of interest exists.

ABSTRACT

Cardiac macrophages are heterogenous in phenotype and functions, which has been associated with differences in their ontogeny. Despite extensive research, our understanding of the precise role of different subsets of macrophages in ischemia/reperfusion injury remains incomplete. We here investigated macrophage lineages and ablated tissue macrophages in homeostasis and after I/R injury in a CSF1R-dependent manner. Genomic deletion of a fms-intronic regulatory element (FIRE) in the Csf1r locus resulted in specific absence of resident homeostatic and antigen-presenting macrophages, without affecting the recruitment of monocyte-derived macrophages to the infarcted heart. Specific absence of homeostatic, monocyte-independent macrophages altered the immune cell crosstalk in response to injury and induced proinflammatory neutrophil polarization, resulting in impaired cardiac remodelling without influencing infarct size. In contrast, continuous CSF1R inhibition led to depletion of both resident and recruited macrophage populations. This augmented adverse remodelling after I/R and led to an increased infarct size and deterioration of cardiac function. In summary, resident macrophages orchestrate inflammatory responses improving cardiac remodelling, while recruited macrophages determine infarct size after I/R injury. These findings attribute distinct beneficial effects to different macrophage populations in the context of myocardial infarction.

GRAPHICAL ABSTRACT

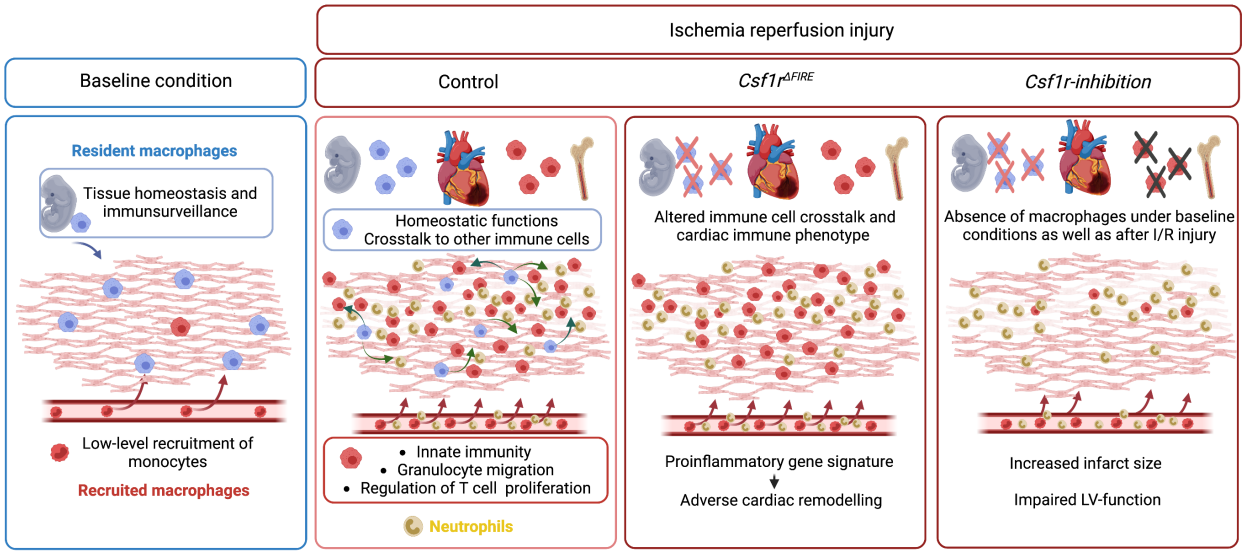

INTRODUCTION

Macrophages are important effectors of innate immunity. They are essential for host defense against infections but are also involved in different cardiovascular diseases. They represent the most abundant immune cell population in healthy cardiovascular tissues (Heidt *et al*, 2014; Weinberger *et al*, 2020), where they contribute to organ functions (Hulsmans *et al*, 2017) and maintenance of tissue homeostasis (Nicolas-Avila *et al*, 2020). In cardiovascular diseases such as atherosclerosis and its main sequelae, ischemic stroke and acute myocardial infarction (AMI), macrophage functions are central to both disease development and healing. AMI has remained a leading cause of mortality and morbidity worldwide (Ahmad & Anderson, 2021; Lozano *et al*, 2012). Although acute survival in this condition has improved through the broad availability of percutaneous coronary intervention, adverse myocardial remodeling and fibrosis frequently result in heart failure (Gerber *et al*, 2016). Pathophysiologically, the diminished blood supply to myocardial tissue during AMI leads to acute tissue necrosis, which induces a profound sterile inflammation and triggers complex cascade of immune processes and tissue remodeling (Hilgendorf *et al*, 2014; Honold & Nahrendorf, 2018; Nahrendorf *et al*, 2007). Consequently, uncontrolled immune reactions in the course of AMI are associated with impaired wound healing and adverse remodeling and can result in worsened cardiac outcome (Panizzi *et al*, 2010).

Macrophages play an essential role in cardiac injury, and thus represent a potential therapeutic target (Hilgendorf *et al.*, 2014; Nahrendorf *et al.*, 2007). However, they are an heterogeneous population (Kubota *et al*, 2019; Weinberger & Schulz, 2015; Zaman & Epelman, 2022), and a large body of work has shown that they can have both pro- and anti-inflammatory functions. The differential roles of macrophage populations in AMI have remained incompletely understood. Cardiac macrophages can derive from embryonic and adult hematopoietic progenitors

87 (Epelman *et al*, 2014). Fate mapping analyses have identified yolk sac (YS) erythro-myeloid
88 progenitors (EMPs) as a principal source of cardiac macrophages in adult life (Ginhoux *et al*,
89 2010). However, limited labeling in inducible cre reporter systems have not allowed for precisely
90 differentiating and quantifying developmental origins of cardiac macrophages. Further, targeting
91 of these macrophages has been challenging (Frieler *et al*, 2015; Ruedl & Jung, 2018).

92 In this study, we investigated the cellular identity of cardiac macrophages in association
93 with their developmental paths and their immune responses to ischemia/reperfusion (I/R) injury.
94 By combining lineage tracing with single cell RNA sequencing, we provide an in-depth analysis
95 of the differential functions of resident and recruited cardiac macrophages. We then harnessed
96 mice with genomic deletion of the fms-intronic regulatory element (FIRE) (Rojo *et al*, 2019), that
97 allowed us to specifically address populations of resident macrophages in the infarcted heart and
98 compared them to mice, in which both recruited as well as resident macrophages are depleted by
99 pharmacological inhibtion of the CSF1R-signalling pathway. Using these approaches of selective
100 macrophage depletion, we could attribute different beneficial functions to resident and also to
101 recruited macrophages which impact differently on cardiac remodeling, infarct size and cardiac
102 outcome.
103

RESULTS

Absence of resident cardiac macrophages in Csf1r$^{\Delta FIRE}$ mice

To quantify the contribution of YS EMPs to cardiac resident macrophages, we harnessed constitutive labeling in *Rank*^{Cre};*Rosa26*^{eYFP} mice (Jacome-Galarza *et al*, 2019; Mass *et al*, 2016; Percin *et al*, 2018). ~80% of cardiac macrophages expressed YFP in hearts of 12 week-old animals, whereas blood monocytes were not labeled (**Fig 1A; Fig S1)**. EMP-derived microglia served as control confirming high efficiency of Cre-mediated recombination. In a comparative analysis, we traced fetal and adult definitive hematopoiesis in *Flt3^{Cre}Rosa26^{eYFP}* mice (Gomez Perdiguero *et al*, 2015; Schulz *et al*, 2012), indicating that ~20% of cardiac macrophages derived from definitive HSC **(Fig 1B)**. Thus, the majority of resident macrophages in the healthy heart is of early embryonic origin.

To determine the role of resident macrophages in the mouse heart, we generated *Rank^{Cre}Rosa26^{DTR}* mice that express the avian diphtheria toxin (DT) receptor in the EMP lineage, rendering them susceptible to DT-mediated ablation. Administration of a single DT dose, however, resulted in premature death of all mice (n=6) within 24 hours (**Fig S2**). The injected mice presented with a systemic inflammatory response syndrome (SIRS)-like phenotype, indicating that acute depletion of EMP-derived macrophages is not viable.

In *Csf1r$^{\Delta FIRE}$* mice, genetic deletion of the fms-intronic regulatory element (FIRE) in the first intron of the *Csf1r* gene leads to a selective absence of tissue macrophages without the developmental defects observed in *Csf1r$^{-/-}$* mice (Munro *et al*, 2020; Rojo *et al.*, 2019). We first confirmed that cardiac macrophages in *Csf1r$^{\Delta FIRE/\Delta FIRE}$ mice* (further termed ΔFIRE) mice were reduced by ~90% and the number of monocytes and neutrophils was not altered **(Fig 1C-E)**. We thus crossed the ΔFIRE animals with the YS EMP fate mapping line (*Rank^{Cre}Rosa26^{eYFP}* mice) and showed that

the macrophages absent in ΔFIRE animals were EMP-derived macrophages **(Fig 1F)**, thus offering a new model to investigate the role of resident macrophages in cardiac injury.

Changes in the cardiac immune phenotype in Csf1r$^{\Delta FIRE}$ mice in baseline conditions

To further characterize the macrophage populations absent in healthy hearts of adult ΔFIRE mice, we carried out single cell RNA-sequencing (scRNA-seq) of CD45^{+} immune cells in wildtype, ΔFIRE and *Rank^{Cre}Rosa26^{eYFP}* mice **(Fig 2A, Fig S3)**. We identified the presence of six macrophage clusters in control mice **(Fig 2B, Fig S3)**. Two clusters of macrophages expressing homeostatic (*e.g. Lyve-1, Gas6, Stab1*) and antigen presentation-related genes (*e.g. CD74, H2-Ab1*) were specifically ablated in ΔFIRE mice **(Fig 2C)**, which largely represent YFP-expressing macrophages in *Rank^{Cre}Rosa26^{eYFP}* mice **(Fig 2D).** Specifically, we mapped ~90% of *yfp* transcripts to the two clusters of homeostatic and antigen presenting macrophages that were ablated in ΔFIRE. Other clusters were not reduced in ΔFIRE, and also were not quantitatively represented in the YS macrophage lineage tracing model, i.e. *Cx3cr1^{hi}* (2% *yfp*), *Ccr2^{low}Ly6c^{lo}* (5% *yfp*) and *Ccr2^{hi}Ly6c^{hi}* (1% *yfp*) macrophages within respective clusters (**Fig 2D**). The specific impact of ΔFIRE on resident macrophages is further supported by the observation, that no changes in gene expression nor cell numbers were observed in *Ly6c^{hi}* monocytes and inflammatory *Ccr2^{hi}Ly6c^{hi}* macrophages **(Fig 2C Fig S4)**. Together, ΔFIRE allows for investigating the role of resident cardiac macrophages that are largely of YS origin.

Absence of resident macrophages in ΔFIRE was associated with changes in gene expression in non-macrophage clusters such as *T- and B-cells* and *natural killer (NK)* cells (**Fig S5**). Further, overall phagocytic capacity, as inferred by expression of phagocytosis related genes (Amorim *et al*, 2022), was reduced (**Fig 2E**). This suggests that absence of resident macrophages is accompanied by distinct changes in immune functions in the homeostatic heart.

Adverse cardiac remodeling in Csf1r$^{\Delta FIRE}$ mice after I/R injury

To assess the impact of the absence of resident macrophages in cardiac injury, we subjected ΔFIRE mice to I/R injury and investigated remodeling and functional outcome by sequential positron emission tomography (PET) imaging after 6 and 30 days **(Fig 3A)**. Function of the cardiac left ventricle (LV), as determined by ejection fraction (LVEF) and stroke volume (SV), improved in controls in the course of post-I/R remodeling **(Fig 3B-C)**. In contrast, LVEF and SV remained unchanged or worsened in ΔFIRE mice, and longitudinal observations of mice indicated a negative net effect on ejection fraction from day 6 to day 30 post I/R. Thus, absence of resident macrophages had a negative effect on cardiac remodeling **(Fig 3D-G)**. Nonetheless, infarct size as determined by viability defect (PET) and fibrotic area (histology) was not different after 30 days **(Fig 3E-H)**.

Recruitment of BM-derived macrophages into infarct zone of Csf1r$^{\Delta FIRE}$ mice

To gain a deeper understanding of the inflammatory processes taking place in the infarcted heart, we quantified macrophage distribution by immunofluorescence and flow cytometry analysis of ischemic and remote areas after I/R. In ΔFIRE mice, macrophages were largely absent in the remote zone of infarcted hearts **(Fig 4A)**, indicating sustained depletion of resident macrophages. However, macrophages strongly increased in the infarct area and their numbers were not different in both infarct and border zones between ΔFIRE and control mice **(Fig 4A)**. This indicated recruitment and differentiation of ΔFIRE-independent macrophages from the circulation into these regions. Indeed, complementing lineage tracing of BM HSC in *Flt3^{Cre}* mice (**Fig 4B**) and YS EMP in *Rank^{Cre}* mice (**Fig 4C**) proved the recruitment of macrophages from BM HSC (Flt3 GFP+ and Rank RFP-, respectively) in the early phase of I/R injury. 30 days after I/R, BM-derived macrophages remained overrepresented in the infarct zone (~75% HSC contribution), and differential contribution of BM HSC declined from the border zone (~50%) to the remote zone

(~35%) **(Fig 4D)**. Taken together, recruited BM-derived macrophages represent the main population in the infarct area and their recruitment was unaltered in ΔFIRE mice. This supports the notion that resident macrophages influence cardiac remodeling but recruited macrophages drive infarct size after I/R.

Transcriptional landscape of resident versus recruited macrophages in I/R injury

To address the differential responses of resident and recruited macrophages to I/R injury, we generated BM chimeric mice. We applied an irradiation-independent model using conditional deletion of c-myb to deplete BM hematopoietic cells in CD45.2 mice and replace them with CD45.1 donor HSC. 2 days after I/R injury, we FACS-sorted recruited ($CD45.1^+$) and resident ($CD45.2^+$) macrophages and carried out bulk RNA sequencing **(Fig 5A)**. The two macrophage populations exhibited profound transcriptional differences after I/R injury. Expression of homeostasis-related genes like *Timd4, Lyve-1, CD163* and *Retnla* was increased in resident $CD45.2^+$ macrophages **(Fig 5B, C).** Substantiating the differential regulation of macrophage programs, $CD45.1^+$ macrophages increased inflammatory- and host defense-related gene ontology (GO) terms (e.g. myeloid leukocyte related immunity, killing of cells), whereas $CD45.2^+$ macrophages upregulated development- and homeostasis-related GO terms (e.g. extracellular matrix organization, vasculature development, heart muscle development) **(Fig 5D)**. GO enrichment analysis further predicted that processes involved in innate (e.g. leukocyte migration, regulation of defense response, response to bacterium) as well as the adaptive immunity (e.g. T cell selection, T cell activation, B cell proliferation) were increased in $CD45.1^+$ macrophages after infarction **(Fig 5D)**. Thus, resident and recruited macrophages provide distinct transcriptional changes and inferred functions in response to I/R.

Altered inflammatory patterns and immune cell communication in $Csf1r^{\Delta FIRE}$ mice

196 To evaluate the immune response of resident and recruited macrophages to I/R injury in ΔFIRE
197 mice, we interrogated the transcription profile of $CD45^+$ cells from the infarct area **(Fig 6A)**. In
198 contrast to the absence of homeostatic and antigen-presenting macrophage clusters in healthy
199 hearts of ΔFIRE mice **(Fig 2B-C)**, there were less differences in immune cell clusters between
200 ΔFIRE and control mice 2 days after I/R **(Fig 6B, C)**. Abundance of homeostatic macrophages
201 was also reduced at this time point, however, other clusters including *Ccr2^{hi}Ly6c^{hi}* inflammatory
202 macrophages were not altered, which is in line with our histological findings.

203 ΔFIRE was associated with some changes in gene expression in cardiac non-macrophage immune
204 cells. Across different clusters, including lymphocyte and neutrophil clusters, expression of anti-
205 inflammatory genes like *Chil3 (Ym1)* and *Lcn2* was reduced**.** Vice versa, expression of Bcl-family
206 genes like *Blc2a1a* and *Bcl2a1d*, which are associated with apoptosis and inflammatory pathways,
207 was higher in ΔFIRE mice **(Fig S6-8)**. Other upregulated genes were related to antigen presentation
208 (e.g.*CD74, H2-Ab1*), as identified in the *Ccr2^{lo}Ly6c^{lo},* homeostatic and *Ccr2^{hi}Ly6c^{hi}* macrophage
209 clusters **(Fig S6 and 7)**. Further, we interrogated inflammatory gene expression in neutrophils,
210 which are abundant first responders to myocardial infarction. We found that a computed score
211 summing up inflammasome activation (Amorim *et al.*, 2022) was increased in all neutrophil
212 clusters in ΔFIRE mice (**Fig 6D**). Thus, the absence of cardiac macrophages was associated with
213 altered inflammatory properties of non-macrophage immune cells in the infarcted heart.

214 Altered intercellular crosstalk of macrophages is a hallmark of cardiac inflammation. We therefore
215 assessed ligand-receptor (LR) interactions between immune cell populations after I/R injury.
216 Indeed, the number of LR interactions with neutrophils and lymphocytes, as well as the strength
217 of the macrophage-emitted communication signals was markedly reduced in homeostatic, antigen-
218 presenting and *Ccr2^{lo}Ly6c^{lo} Mø* macrophage clusters (**Fig 6E, F)**. In contrast, immune cell

communication in BM-derived macrophage clusters (e.g. *Ccr2^{hi}Ly6c^{hi} Mø cluster,* **Fig S9***)* was not different to control mice. Taken together, deficiency in resident macrophages in I/R injury altered the intercellular immune crosstalk and induced a pro-inflammatory signature in e.g. cardiac neutrophils. However, transcriptional profiles of BM-derived inflammatory macrophages were largely unaltered. Together with our histological analysis showing the dominance of recruited BM-derived macrophages in the early phase of I/R, this potentially explained the limited impact of ΔFIRE on functional outcome after I/R injury.

Ablation of resident and recruited macrophages severely impacts on cardiac healing after I/R injury

To test this hypothesis, we determined the effect of combined ablation of resident and recruited macrophages. We therefore exposed mice to continuous treatment with the CSF1R-inhibitor PLX5622 (**Fig 7A**). In healthy hearts, inhibitor treatment resulted in the absence of cardiac macrophages within 3 days, which had no impact on cardiac function (**Fig S10**). We then subjected mice to I/R injury and investigated outcome by sequential PET imaging and histology **(Fig 7A)**. Treatment with PLX5622 diminished macrophage numbers in both remote and infarct areas in the early phase (day 2) after injury. Recruitment of other myeloid cells e.g. neutrophils was not altered in this context (**Fig 7B**). This effect was pronounced in the chronic phase (day 30) after I/R injury, in which macrophages were largely absent in remote, border and infarct zones (**Fig 7C,D**). Absence of resident and recruited macrophages was associated increased infarct size, as determined by fibrosis area (WGA histology) as well as viability defect (PET), and resulted in deterioration of cardiac function **(Fig 7E-I).** Specifically, LVEF was reduced 6 days after I/R, and remained strongly impaired at 30 days **(Fig 7E).**

241 Taken together, sole absence of resident macrophages had limited negative impact on cardiac
242 remodeling. Absence of both resident and recruited macrophages resulted in a significant increase
243 in infarct size and deterioration of left ventricular function after I/R injury, highlighting a beneficial
244 effect of recruited macrophages in cardiac healing.
245

DISCUSSION

Macrophages are key players in cardiac homeostasis and disease (Bajpai *et al*, 2019; Bajpai *et al*, 2018; Dick *et al*, 2019; Epelman *et al.*, 2014; Hulsmans *et al.*, 2017; Nahrendorf *et al.*, 2007; Nicolas-Avila *et al.*, 2020; Panizzi *et al.*, 2010; Sager *et al*, 2016). The precise understanding of their developmental origin, their functions and their regulation could enable the identification of macrophage-targeted strategies to modify inflammation in the heart. This study sheds light on the differential role of resident and recruited macrophages in cardiac remodeling and outcome after AMI.

BM-derived recruited macrophages are a scarce population in the healthy heart but are recruited in vast numbers to the injured myocardium after I/R injury. These recruited cells exhibit substantially different transcriptional profiles in comparison to their resident counterpart, and show pro-inflammatory properties. Resident macrophages remain present in the remote and border zone and display a reparative gene expression profile after I/R injury. In comparison to recruited macrophages, resident macrophages expressed higher levels of genes related to homeostatic functions (e.g. *Lyve-1, Timd4, CD163, Stab1*). These markers have recently been associated with self-renewing tissue macrophages that are maintained independently of BM contribution (Dick *et al*, 2022). Biological processes associated with cardiac healing are upregulated in resident macrophages (e.g. regulation of vascular development, regulation of cardiomyocyte development, extracellular matrix organization). Transcriptional profiles of recruited macrophages show enhanced inflammatory biological processes also in macrophages harvested from the remote area, underlining their potentially detrimental influence on remote cardiac injury.

Two recent studies addressed the role of resident macrophages using DT-mediated macrophage depletion and reported impaired cardiac remodeling in chronic myocardial infarction

(Dick *et al.*, 2019) and after I/R injury (Bajpai *et al.*, 2019). However, DT-mediated cell ablation is known to induce neutrophil recruitment and tissue inflammation (Frieler *et al.*, 2015; Oh *et al*, 2017; Ruedl & Jung, 2018; Sivakumaran *et al*, 2016). This inflammatory preconditioning of cardiac tissue after DT-depletion is likely to impact on cardiac remodeling and influence assessment of tissue macrophage functions. Genomic deletion of FIRE in the *Csf1r* gene results in the near-absence of resident cardiac macrophages but circumvents the inflammatory stimulus of DT-induced depletion. ΔFIRE specifically diminished homeostatic and antigen-presenting macrophages. Substantiating the specificity to resident cardiac macrophages in this genetic model, the amount of macrophages recruited to the infarct area after I/R injury was not affected in ΔFIRE mice. Further, scRNAseq analysis revealed that gene expression of monocytes as well as *Ccr2*^{hi}*Ly6c*^{hi} *and Cx3cr1*^{hi} Mϕ, representing mainly recruited immune cells, was mostly unchanged in ΔFIRE compared to control mice. The specific targeting of the resident macrophage population introduces an interesting in vivo model for studying their role in MI without the need for inflammation-prone conditional deletion of macrophages (Frieler *et al.*, 2015).

Ablation of resident macrophages altered macrophage crosstalk to non-macrophage immune cells, especially lymphocytes and neutrophils. This was paralleled by a proinflammatory gene signature in neutrophils, with increased expression of inflammasome-related genes and a reduction in anti-inflammatory genes like *Chil3* and *Lcn2* (Gordon & Martinez, 2010; Guo *et al*, 2014; Parmar *et al*, 2018). Interestingly, inflammatory polarization of neutrophils is associated with poor outcome also after ischemic brain injury (Cuartero *et al*, 2013). Consequently, absence of resident macrophages worsened cardiac remodeling in the late postinfarction phase in ΔFIRE mice indicating their biological role in myocardial healing. However, absence of resident macrophages did not change infarct size or impact on LV function.

Depletion of macrophages by pharmacological inhibition of CSF1R induced the absence of both resident and recruited macrophages, allowing us to determine cardiac outcome in juxtaposition to the ΔFIRE mice. Continuous CSF1R inhibition induced the absence of macrophages also in the infarcted area and had deleterious effect on infarct size and LV function. In line with our findings, depletion of macrophages by anti-CSF1R treatment was associated with worsened cardiac function in a model of pressure overload induced heart failure (Revelo *et al*, 2021). Controversially, a recent study in which monocytes were depleted using DT-injections in *Ccr2*^{DTR} mice reported beneficial effects on cardiac outcome after MI in mice. However, other immune cells including neutrophils express CCR2 and may therefore be affected directly (Talbot *et al*, 2015; Xu *et al*, 2017). In line with this, Ccr2-deficient mice exhibit reduced acute recruitment of neutrophils to the brain after I/R injury, which was associated with reduced infarct size and brain edema (Dimitrijevic *et al*, 2007).

Taken together our study underlines the heterogeneity of cardiac macrophages and the importance of ontogeny therein. Resident macrophages, which mainly derive from YS EMPs, govern cardiac homeostasis in the healthy heart, and contribute positively to cardiac healing after I/R injury by orchestrating anti-inflammatory programming of other cardiac immune cells. However, recruited macrophages contribute to the healing phase after AMI and their absence defines infarct size and cardiac outcome.

MATERIALS AND METHODS

Mice

Rank^{Cre} (Jacome-Galarza *et al.*, 2019; Percin *et al.*, 2018), *Flt3*^{Cre} (Benz *et al*, 2008), *Myb*$^{fl/fl}$ (Emambokus *et al*, 2003), *Mx1*^{Cre} (Kuhn *et al*, 1995) (from The Jackson Laboratory (JAX), Stock No: 003556), *Csf1r*$^{\Delta FIRE}$ (Rojo *et al.*, 2019), *Rosa26*^{DTR} (Buch *et al*, 2005) (JAX Stock No: 007900), *Rosa26*$^{mT/mG}$ (Muzumdar *et al*, 2007) (JAX Stock No: 007676), *Rosa26*^{eYFP} (Srinivas *et al*, 2001) (JAX Stock No: 006148), and *Rosa26*^{RFP} (JAX Stock No: 034720) mice have been previously described. PCR genotyping was performed according to protocols described previously. Animals were aged between 10-16 weeks. We have complied with all relevant ethical regulations. Animal studies were approved by the local regulatory agency (Regierung von Oberbayern, Munich, Germany, record numbers ROB-55.2-2532.Vet_02-19-17 and ROB-55.2-2532.Vet_02-19-1; Care and Use Committee of the Institut Pasteur (CETEA), dap190119).

For fate-mapping analysis of Flt3^{+} precursors, *Flt3*^{Cre} males (the transgene is located on the Y chromosome) were crossed to *Rosa26*^{eYFP} or *Rosa26*$^{mT/mG}$ female reporter mice and only the male progeny was used. For all other experiments, the offspring of both sexes was used for experiments.

BM transplantation was enabled by conditional deletion of the transcription factor *myb* as previously described (Stremmel *et al*, 2018). In brief, we induced BM ablation by 4 injections of polyI:C into *CD45.2; Mx1*^{Cre}*Myb*$^{flox/flox}$ every other day, and then transplanted BM from congenic *C57BL/6 CD45.1* (*Ly5.1*; JAX Stock No: 006584). We confirmed the success (chimerism of above 90%) of the BM-transplantation after 4 weeks**.**

To deplete macrophages, we used the selective CSF1R-inhibitor PLX5622. Control and PLX5622 (300 ppm formulated in AIN-76A standard chow, Research Diets, Inc.) chows were kindly provided by Plexxikon Inc (Berkeley, CA). For depletion of RANK-lineage macrophages, *Rank^{Cre}Rosa26^{DTR}* mice were injected intraperitoneally with 0.02 mg/kg body weight diphtheria toxin (DT; Sigma-Aldrich) at the timepoints mentioned in Fig ure and corresponding legend. Mice were closely monitored by veterinarians and according to score sheets that were approved by the regulatory agency. Single DT application in *Rank^{Cre}Rosa26^{DTR}* mice let to rapid deterioration of their health (without infarction or other interventions), and consequently experiments needed to be aborted according to regulations; experimental outcomes were then documented as premature death as indicated.

Ischemia-reperfusion (I/R) injury

I/R injury was carried out as previously described (Nicolas-Avila *et al.*, 2020). In brief, mice were anesthetized using 2% isoflurane and intraperitoneal injection of fentanyl (0.05 mg/kg), midazolam (5.0 mg/kg) and medetomidine (0.5 mg/kg), and then intubated orally (MiniVent Ventilator model nr. 845, Harvard Apparatus®) and ventilated (volume of 150 µL at 200/min). After lateral thoracotomy, the left anterior descending artery (LAD) was ligated with an 8-0 prolene suture producing an ischemic area in the apical left ventricle (LV). To induce the reperfusion injury, the suture was removed after 60 min and reperfusion was confirmed by observing the recoloring of the LV. For experiments with CD169-DTR mice, animals were anesthetized with xylazine and ketamine, and duration of ischemia was 45 min in the I/R model as described earlier (Nicolas-Avila *et al.*, 2020). Postoperative analgesia was performed by injection of Buprenorphin (0.1 mg/kg) twice per day for 3 days. After 2, 6 or 30 days after I/R injury organs were harvested after cervical dislocation.

Organ harvest

Mice were anaesthetized using 2% isoflurane and organ harvest was performed after cervical dislocation. Blood was harvested with a heparinized syringe (2mL) by cardiac puncture. After perfusion with 20 mL of ice-cold PBS hearts were excised and kept in PBS on ice until further tissue processing. For flow cytometry, hearts were divided into the ischemia (tissue distal of the LAD ligation) and remote area (tissue proximal of the LAD ligation). For histological examinations of tissues, hearts were incubated in 4% PFA for 30 min followed by an incubation in 30% sucrose-solution (Sigma Aldrich®) for 24 h. Afterwards, hearts were mounted onto a heart slicing device and cut transversally into 3 equal parts (termed level 1, 2 and 3) and stored in Tissue-Tek® (Sakura Finetek Germany GmbH) at -80°C.

Immunohistology

Cryosections (10-12 µm) of heart tissue were fixed with 4% paraformaldehyde for 10 min. Blocking and permeabilization were performed with 0.5% Saponin and 10% goat serum for 1h. Primary antibodies were added and incubated for 2-18 h (see Supplemental Table 1). Slides were washed with PBS and secondary antibodies were added and incubated for 1h (see Supplemental Table 1). WGA-staining (Wheat Germ Agglutinin Alexa Fluor™ 647 conjugated antibody, ThermoFisher Scientific®) was used to locate and measure the infarct area and nuclei were stained with DAPI. Finally, slides were washed one more time and Fluorescence Mounting Medium was used to cover the stained sample.

Heart samples were evaluated using an Axio Imager M2 (Carl Zeiss®) and blinded picture analysis was performed using ZEN Imaging and Axiovision SE64 Rel. 4.9.1 (Carl Zeiss®). For the evaluation of cell numbers, 6 individual high-resolution images from each respective anatomical region (infarct area, border zone and remote zone) were analysed for each animal. To

measure infarct size the heart was cut into 3 parts and the infarcted area was measured as WGA^+ area in sections from each part.

Flow cytometry

100 µL of heparinized blood was used for FACS analysis. Erythrocytes were lysed with 1% ammonium chloride. After washing with PBS, the cell suspension was resuspended in purified rat anti-mouse CD16/CD32 (BD Pharmingen®) and incubated for 15 min at 4°C. Following this, cells were incubated with FACS-antibodies for 15 min at 4°C **(table S1)**.

Heart tissue was dissected into remote and ischemic tissue as described above and minced into small pieces using forceps and a scalpel. When comparing baseline and I/R injury in FACS analysis, basal heart tissue was used for comparison with remote tissue and apical heart tissue for comparison with ischemia tissue. After enzymatic digestion (Collagenase XI 1200 U/mg, Collagenase I 125 U/mg, Hyaluronidase 500 U/mg, DNase I 1836 U/mg; Sigma Aldrich®) for 30 min at 37°C cells were washed and incubated with purified anti-CD16/32 (FcγRIII/II; dilution 1/50) for 10 min. Thereafter, cells were incubated wit FACS-antibodies (**table S1**) for 30 min at 4°C. FACS-analysis was performed on a BD Fortessa® or a BeckmanCoulter Cytoflex® flow cytometer and gating strategies are shown in Supplemental Fig ures 1 and 3. Data were analysed using FlowJo® (version 10.0.8r1).

Cell Sorting

Cell sorting was performed on a MoFlo Astrios (Beckman Coulter) to obtain cardiac macrophages from *CD45.2; Mx1^{Cre}Myb$^{flox/flox}$* after BM-transplantation of CD45.1 BM (n=3 for 2 days after I/R injury) for bulk sequencing, or all cardiac immune cells ($CD45^+$ cells) of *Csf1r$^{\Delta FIRE}$* and *Rank^{Cre}Rosa26^{eYFP}* mice (n=3 for *Csf1r$^{\Delta FIRE/+}$* and *Csf1r$^{\Delta FIRE/\Delta FIRE}$* in baseline conditions, n=1

for *Rank*^{Cre}*Rosa26*^{eYFP} in baseline conditions; n=2 for *Csf1r*$^{\Delta FIRE/+}$ and *Csf1r*$^{\Delta FIRE/\Delta FIRE}$ 2 days after I/R injury) for single cell analysis. CD45$^+$ cells were enriched by using magnetic beads and MS columns (CD45 MicroBeads; Miltenyi Biotec). Cells were then sorted as single/live/CD45$^+$ cells for single cell sequencing from baseline hearts and from the ischemic myocardium 2 days after I/R injury. Bulk sequencing was performed on single/live/CD45$^+$/lin$^-$/CD11b$^+$/F4/80$^+$/CD64$^+$/CD45.1$^+$ or CD45.2$^+$ cells from the remote and the ischemic myocardium 2 days after I/R injury. Dead cells were identified with SYTOX Orange Dead Cell Stain.

Bulk sequencing and analysis

For each sample, ~1000 macrophages were sorted into 75µL of RLT buffer (Qiagen, containing 1% beta-mercaptoethanol), vortexed for 1 min and immediately frozen (-80°C). RNA extraction (RNeasy® Plus Micro Kit, Qiagen), cDNA generation (SMART®-Seq v4 Ultra Low Input RNA Kit, Takara Bio) and library preparation (Nextera® XT DNA Library Prep Kit, Illumina) were performed according to the manufacturer's specifications. Sequencing was performed on a HiSeq4000 system (Ilumina).

The obtained reads were trimmed using bbduk from the BBMap (https://sourceforge.net/projects/bbmap/) v38.87 collection using parameters "ktrim=r k=23 mink=11 hdist=1 tpe tbo". The trimmed reads were aligned with Hisat2 2.2.1 against the Ensembl release 102 reference mouse genome (Yates *et al*, 2020).

Gene expression was quantified using the featureCounts (Liao *et al*, 2014) application from the subread package (v2.0.1) and with parameters "--primary -O -C -B -p -T 8 --minOverlap 5". Differential expression analysis was performed using DESeq2 (v1.30.0) (Love *et al*, 2014). A Gene Ontology Set Enrichment analysis was performed using the ClusterProfiler R package (v3.18.1). The visualization of the respective clustermaps was layouted using the ForceAtlas2

implementation of the python fa2 (https://pypi.org/project/fa2/) package for networkx (v2.5) (https://networkx.org/).

On the library-size normalized count data, the pymRMR ((Peng *et al*, 2005), https://pypi.org/project/pymrmr/) package was used to derive the top 100 discriminatory genes (Mutual Information Quotient method) for subsequently calculating the UMAP 2D-embedding ((McInnes *et al*, 2020), (https://pypi.org/project/umap-learn/)) for all samples (umap-learn package v0.5.0rc1, 3 neighbors) ((McInnes *et al*, 2018), https://pypi.org/project/pymrmr/).

Single cell RNA sequencing and analysis

After sorting, cells were proceeded for single cell capture, barcoding and library preparation using Chromium Next GEM single cell 3' (v3.1, 10x Genomics) according to manufacturer's specifications. Pooled libraries were sequenced on an Illumina HiSeq1500 sequencer (Illumina, San Diego, USA) in paired-end mode with asymmetric read length of 28+91 bp and a single indexing read of 8bp.

The reads of heart1 sample ($Rank^{Cre}Rosa26^{eYFP}$) were demultiplexed using Je-demultiplex-illu (Girardot *et al*, 2016) and mapped against a customized mouse reference genome (GRCm38.p6, Gencode annotation M24) including eYfp sequence using CellRanger (v3.1.0, 10x Genomics).

The six mouse samples 20133-0001 to 20133-0006 (baseline condition of $Csf1r^{\Delta FIRE/+}$ and $Csf1r^{\Delta FIRE/\Delta FIRE}$), were processed using Cellranger 4.0.0 using the 2020A mm10 reference.

The 4 mouse samples (MUC13956-13959, infarct condition of $Csf1r^{\Delta FIRE/+}$ and $Csf1r^{\Delta FIRE/\Delta FIRE}$), were sequenced with 4 technical sequencing replicates and pooled using the

cellranger (v4.0.0, 10x Genomics) pipeline. Cellranger 4.0.0 was called with default parameters and the 2020A mm10 reference for gene expression.

Finally, all 11 samples were integrated using Seurat 4.0.0 (on R 4.0.1) (Stuart & Satija, 2019). The samples were processed, and cells were filtered to contain between 200 and 6000 features, have at least 1000 molecules detected (nCount_RNA > 1000), have below 15% mtRNA content (^MT) and below 40% ribosomal RNA content (^Rps|^Rpl). After this filtering a total of 35759 cells remained.

After performing SCTransform (Hafemeister & Satija, 2019) on the samples, the SCTransform vignette for integrating the datasets was followed (with 2000 integration features). For dimensionality reduction, PCA was performed using default parameters, and UMAP and Neighbour-Finding was run on 50 PCs. Clustering was performed at a resolution of 0.8. A total of 18 clusters was identified using this approach. Cluster markers were calculated using the t-test in the FindMarkers function. Subsequently cell types were initially predicted using the cPred cell type prediction (https://github.com/mjoppich/scrnaseq_celltype_prediction). Upon manual curation, further fine-grained cell type annotations were made. Differential comparisons were performed against several subgroups of the data set. These comparisons were performed using the t-test in the FindMarkers function of Seurat. Differential results are visualized using the EnhancedVolcano library (Blighe K, 2021).

For the analysis of cell-cell interactions we downloaded the ligand-receptor pairs from Jin et al. (Jin *et al*, 2021) from the Lewis Lab GitHub repository (https://github.com/LewisLabUCSD/Ligand-Receptor-Pairs). For each interaction (ligand-receptor pair for a cluster-pair) the communication score is calculated as the expression product (Armingol *et al*, 2021) of the mean normalized expressions exported from the Seurat object. This

ensures that little expression of either ligand or receptor in only one cluster results in a relatively low communication score, and only good expression of ligand and receptor will result in a high communication score. The direction of an interaction is fixed from ligand to receptor. The single ligand-receptor-communication-scores were then aggregated (sum) such that only interactions with a score greater six were taken into account.

Gene module scores for inflammasome, ROS and phagocytosis gene sets were calculated using Seurat's AddModuleScore function. All scripts, including the ones for creating the visualizations of bulk and scRNA-seq data, are available online through https://github.com/mjoppich/myocardial_infarction .

In Vivo PET Imaging

ECG-gated positron emission tomography (PET) images were performed on day 6 and 30 after I/R injury of the LAD using a dedicated small-animal PET scanner (Inveon Dedicated PET, Preclinical Solutions, Siemens Healthcare Molecular Imaging, Knoxville, TN, USA), as previously described (Brunner *et al*, 2012). Anaesthesia was induced with isoflurane (2.5%), delivered via a face mask in pure oxygen at a rate of 1.2 L/min and maintained with isoflurane (1.5%). Approximately 15 MBq 2-deoxy-2-[18F]fluoro-D-glucose ([18F]-FDG) (~100 µL) were administered through a teil vein catheter and slowly flushed immediately afterwards with 50 µL saline solution. Body temperature was monitored using a rectal thermometer and maintained within the normal range using a heating pad. After placing animals within the aperture of the PET scanner ECG electrodes (3M, St. Paul, MN, USA) were placed on both forepaws and the left hind paw and ECG was recorded using a dedicated physiological monitoring system (BioVet; Spin Systems Pty Ltd., Brisbane, Australia) (Todica *et al*, 2018). The PET emission acquisition (list-mode) was initiated 30 min after [18F]-FDG injection and lasted 15 min (Brunner *et al.*, 2012;

Gross *et al*, 2016). For scatter and attenuation correction and additional 7-min long transmission scan was performed using a Co-57 source.

The accuracy of the ECG trigger signal was verified retrospectively using in-house software programmed in MATLAB (The Mathworks, Natick, USA) and in C programming language and erroneous trigger events were removed when needed, as previously described (Boning *et al*, 2013). Further processing of the data was performed using the Inveon Acquisition Workplace (Siemens Medical Solutions, Knoxville, TN). As previously described, data was reconstructed as a static image or as a cardiac gated image with 16 bins in a 128 × 128 matrix with a zoom of 211% using an OSEM 3D algorithm with 4 and a MAP 3D algorithm with 32 iterations (Brunner *et al.*, 2012). The reconstructed data was normalized, corrected for randoms, dead time and decay as well as attenuation and scatter.

PET images were analysed using the Inveon Research Workplace in a blinded manner (Siemens Medical Solutions, Knoxville, TN). Infarct sizes were determined from static reconstructed images using QPS® (Cedars-Sinai, Los Angeles, CA, USA). Hereby, datasets were compared to a normative database and the viability defect was calculated as percentage of the left ventricular volume, as described previously (Lehner *et al*, 2014; Todica *et al*, 2014). Left ventricular function volumes (EDV, ESV, SV), as well as the LVEF, were determined from ECG-gated images using QGS® (Cedars-Sinai, Los Angeles, CA, USA), as described previously (Brunner *et al.*, 2012; Croteau *et al*, 2003).

Statistical analysis

Student's t-test or Fisher's LSD test was used (Prism GraphPad®). Welch's correction for unequal variances was used when applicable. A p-value of $p < 0.05$ was considered significant. Data are presented as mean +/- standard deviation (SD).

514

ACKNOLEDGEMENTS

We thank Nicole Blount, Beate Jantz, Michael Lorenz, Sebastian Helmer for excellent technical assistance.

FUNDING:

DZHK (German Centre for Cardiovascular Research) and the BMBF (German Ministry of Education and Research) (grants 81Z0600204 to CS, 81X2600252 to TW and 81X2600256 to MF). The Deutsche Forschungsgemeinschaft (SCHU 2297/1-1 and collaborative research centers 1123 project Z02 (MJ, RZ) and A07 (CS), and CRC TRR332 project A6 (CS). LMUexcellent (TW). ESC Research Grant 2021 (TW). Friedrich-Baur Stiftung (TW). Deutsche Stiftung für Herzforschung (M.F.). Chinese Scholarship Council (CSC) to JF and LL.

AUTHOR CONTRIBUTIONS:

Conceptualization: TW, CSchu

Methodology: TW, MJ, MF, JL, GP, AT, DE, CSchu

Investigation: TW, DM, MJ, MF, CG, KK, VW, SR, SA, JF, LL, WHL, JW, LT, DE, GP, SMS

Funding acquisition: TW, MF, RZ, EGP, CSchu

Supervision: AH, CW, SE, AT, RZ, CP, EGP, CSchu

Writing – original draft: TW, MJ

Writing – review & editing: all authors

Conflict of interest:

The authors declare no conflict of interest.

References

Ahmad FB, Anderson RN (2021) The Leading Causes of Death in the US for 2020. *JAMA*

Amorim A, De Feo D, Friebel E, Ingelfinger F, Anderfuhren CD, Krishnarajah S, Andreadou M, Welsh CA, Liu Z, Ginhoux F *et al* (2022) IFNgamma and GM-CSF control complementary differentiation programs in the monocyte-to-phagocyte transition during neuroinflammation. *Nat Immunol* 23: 217-228

Armingol E, Officer A, Harismendy O, Lewis NE (2021) Deciphering cell-cell interactions and communication from gene expression. *Nat Rev Genet* 22: 71-88

Bajpai G, Bredemeyer A, Li W, Zaitsev K, Koenig AL, Lokshina I, Mohan J, Ivey B, Hsiao HM, Weinheimer C *et al* (2019) Tissue Resident CCR2- and CCR2+ Cardiac Macrophages Differentially Orchestrate Monocyte Recruitment and Fate Specification Following Myocardial Injury. *Circ Res* 124: 263-278

Bajpai G, Schneider C, Wong N, Bredemeyer A, Hulsmans M, Nahrendorf M, Epelman S, Kreisel D, Liu Y, Itoh A *et al* (2018) The human heart contains distinct macrophage subsets with divergent origins and functions. *Nat Med* 24: 1234-1245

Benz C, Martins VC, Radtke F, Bleul CC (2008) The stream of precursors that colonizes the thymus proceeds selectively through the early T lineage precursor stage of T cell development. *J Exp Med* 205: 1187-1199

Blighe K RS, Lewis M, 2021. EnhancedVolcano: Publication-ready volcano plots with enhanced colouring and labeling. R package version 1.10.0, https://githubcom/kevinblighe/EnhancedVolcano

Boning G, Todica A, Vai A, Lehner S, Xiong G, Mille E, Ilhan H, la Fougere C, Bartenstein P, Hacker M (2013) Erroneous cardiac ECG-gated PET list-mode trigger events can be retrospectively identified and replaced by an offline reprocessing approach: first results in rodents. *Phys Med Biol* 58: 7937-7959

Brunner S, Todica A, Boning G, Nekolla SG, Wildgruber M, Lehner S, Sauter M, Ubleis C, Klingel K, Cumming P *et al* (2012) Left ventricular functional assessment in murine models of ischemic and dilated cardiomyopathy using [18 F]FDG-PET: comparison with cardiac MRI and monitoring erythropoietin therapy. *EJNMMI Res* 2: 43

Buch T, Heppner FL, Tertilt C, Heinen TJ, Kremer M, Wunderlich FT, Jung S, Waisman A (2005) A Cre-inducible diphtheria toxin receptor mediates cell lineage ablation after toxin administration. *Nat Methods* 2: 419-426

Croteau E, Benard F, Cadorette J, Gauthier ME, Aliaga A, Bentourkia M, Lecomte R (2003) Quantitative gated PET for the assessment of left ventricular function in small animals. *J Nucl Med* 44: 1655-1661

Cuartero MI, Ballesteros I, Moraga A, Nombela F, Vivancos J, Hamilton JA, Corbi AL, Lizasoain I, Moro MA (2013) N2 neutrophils, novel players in brain inflammation after stroke: modulation by the PPARgamma agonist rosiglitazone. *Stroke* 44: 3498-3508

Dick SA, Macklin JA, Nejat S, Momen A, Clemente-Casares X, Althagafi MG, Chen J, Kantores C, Hosseinzadeh S, Aronoff L *et al* (2019) Self-renewing resident cardiac macrophages limit adverse remodeling following myocardial infarction. *Nat Immunol* 20: 29-39

Dick SA, Wong A, Hamidzada H, Nejat S, Nechanitzky R, Vohra S, Mueller B, Zaman R, Kantores C, Aronoff L *et al* (2022) Three tissue resident macrophage subsets coexist across organs with conserved origins and life cycles. *Sci Immunol* 7: eabf7777

Dimitrijevic OB, Stamatovic SM, Keep RF, Andjelkovic AV (2007) Absence of the chemokine receptor CCR2 protects against cerebral ischemia/reperfusion injury in mice. *Stroke* 38: 1345-1353

Emambokus N, Vegiopoulos A, Harman B, Jenkinson E, Anderson G, Frampton J (2003) Progression through key stages of haemopoiesis is dependent on distinct threshold levels of c-Myb. *EMBO J* 22: 4478-4488

Epelman S, Lavine KJ, Beaudin AE, Sojka DK, Carrero JA, Calderon B, Brija T, Gautier EL, Ivanov S, Satpathy AT *et al* (2014) Embryonic and adult-derived resident cardiac macrophages are maintained through distinct mechanisms at steady state and during inflammation. *Immunity* 40: 91-104

Frieler RA, Nadimpalli S, Boland LK, Xie A, Kooistra LJ, Song J, Chung Y, Cho KW, Lumeng CN, Wang MM *et al* (2015) Depletion of macrophages in CD11b diphtheria toxin receptor mice induces brain inflammation and enhances inflammatory signaling during traumatic brain injury. *Brain Res* 1624: 103-112

Gerber Y, Weston SA, Enriquez-Sarano M, Berardi C, Chamberlain AM, Manemann SM, Jiang R, Dunlay SM, Roger VL (2016) Mortality Associated With Heart Failure After Myocardial Infarction: A Contemporary Community Perspective. *Circ Heart Fail* 9: e002460

Ginhoux F, Greter M, Leboeuf M, Nandi S, See P, Gokhan S, Mehler MF, Conway SJ, Ng LG, Stanley ER *et al* (2010) Fate mapping analysis reveals that adult microglia derive from primitive macrophages. *Science* 330: 841-845

Girardot C, Scholtalbers J, Sauer S, Su SY, Furlong EE (2016) Je, a versatile suite to handle multiplexed NGS libraries with unique molecular identifiers. *BMC Bioinformatics* 17: 419

Gomez Perdiguero E, Klapproth K, Schulz C, Busch K, Azzoni E, Crozet L, Garner H, Trouillet C, de Bruijn MF, Geissmann F *et al* (2015) Tissue-resident macrophages originate from yolk-sac-derived erythro-myeloid progenitors. *Nature* 518: 547-551

Gordon S, Martinez FO (2010) Alternative activation of macrophages: mechanism and functions. *Immunity* 32: 593-604

Gross L, Paintmayer L, Lehner S, Brandl L, Brenner C, Grabmaier U, Huber B, Bartenstein P, Theiss HD, Franz WM *et al* (2016) FDG-PET reveals improved cardiac regeneration and attenuated adverse remodelling following Sitagliptin + G-CSF therapy after acute myocardial infarction. *Eur Heart J Cardiovasc Imaging* 17: 136-145

Guo H, Jin D, Chen X (2014) Lipocalin 2 is a regulator of macrophage polarization and NF-kappaB/STAT3 pathway activation. *Mol Endocrinol* 28: 1616-1628

Hafemeister C, Satija R (2019) Normalization and variance stabilization of single-cell RNA-seq data using regularized negative binomial regression. *Genome Biol* 20: 296

Heidt T, Courties G, Dutta P, Sager HB, Sebas M, Iwamoto Y, Sun Y, Da Silva N, Panizzi P, van der Laan AM *et al* (2014) Differential contribution of monocytes to heart macrophages in steady-state and after myocardial infarction. *Circ Res* 115: 284-295

Hilgendorf I, Gerhardt LM, Tan TC, Winter C, Holderried TA, Chousterman BG, Iwamoto Y, Liao R, Zirlik A, Scherer-Crosbie M *et al* (2014) Ly-6Chigh monocytes depend on Nr4a1 to balance both inflammatory and reparative phases in the infarcted myocardium. *Circ Res* 114: 1611-1622

Honold L, Nahrendorf M (2018) Resident and Monocyte-Derived Macrophages in Cardiovascular Disease. *Circ Res* 122: 113-127

Hulsmans M, Clauss S, Xiao L, Aguirre AD, King KR, Hanley A, Hucker WJ, Wulfers EM, Seemann G, Courties G *et al* (2017) Macrophages Facilitate Electrical Conduction in the Heart. *Cell* 169: 510-522 e520

Jacome-Galarza CE, Percin GI, Muller JT, Mass E, Lazarov T, Eitler J, Rauner M, Yadav VK, Crozet L, Bohm M *et al* (2019) Developmental origin, functional maintenance and genetic rescue of osteoclasts. *Nature* 568: 541-545

Jin S, Guerrero-Juarez CF, Zhang L, Chang I, Ramos R, Kuan CH, Myung P, Plikus MV, Nie Q (2021) Inference and analysis of cell-cell communication using CellChat. *Nat Commun* 12: 1088

Kubota A, Suto A, Suzuki K, Kobayashi Y, Nakajima H (2019) Matrix metalloproteinase-12 produced by Ly6C(low) macrophages prolongs the survival after myocardial infarction by preventing neutrophil influx. *J Mol Cell Cardiol* 131: 41-52

Kuhn R, Schwenk F, Aguet M, Rajewsky K (1995) Inducible gene targeting in mice. *Science* 269: 1427-1429

Lehner S, Todica A, Vanchev Y, Uebleis C, Wang H, Herrler T, Wangler C, Cumming P, Boning G, Franz WM *et al* (2014) In vivo monitoring of parathyroid hormone treatment after myocardial infarction in mice with [68Ga]annexin A5 and [18F]fluorodeoxyglucose positron emission tomography. *Mol Imaging* 13: 1-8

Liao Y, Smyth GK, Shi W (2014) featureCounts: an efficient general purpose program for assigning sequence reads to genomic features. *Bioinformatics* 30: 923-930

Love MI, Huber W, Anders S (2014) Moderated estimation of fold change and dispersion for RNA-seq data with DESeq2. *Genome Biol* 15: 550

Lozano R, Naghavi M, Foreman K, Lim S, Shibuya K, Aboyans V, Abraham J, Adair T, Aggarwal R, Ahn SY *et al* (2012) Global and regional mortality from 235 causes of death for 20 age groups in 1990 and 2010: a systematic analysis for the Global Burden of Disease Study 2010. *Lancet* 380: 2095-2128

Mass E, Ballesteros I, Farlik M, Halbritter F, Gunther P, Crozet L, Jacome-Galarza CE, Handler K, Klughammer J, Kobayashi Y *et al* (2016) Specification of tissue-resident macrophages during organogenesis. *Science* 353

McInnes L, Healy J, Melville J (2020) UMAP: Uniform Manifold Approximation and Projection for Dimension Reduction. *arXiv*

McInnes L, Healy J, Saul N, Großberger L (2018) UMAP: Uniform Manifold Approximation and Projection. *J Open Source Softw* 3, (29), 861

Munro DAD, Bradford BM, Mariani SA, Hampton DW, Vink CS, Chandran S, Hume DA, Pridans C, Priller J (2020) CNS macrophages differentially rely on an intronic Csf1r enhancer for their development. *Development* 147

Muzumdar MD, Tasic B, Miyamichi K, Li L, Luo L (2007) A global double-fluorescent Cre reporter mouse. *Genesis* 45: 593-605

Nahrendorf M, Swirski FK, Aikawa E, Stangenberg L, Wurdinger T, Fig ueiredo JL, Libby P, Weissleder R, Pittet MJ (2007) The healing myocardium sequentially mobilizes two monocyte subsets with divergent and complementary functions. *J Exp Med* 204: 3037-3047

Nicolas-Avila JA, Lechuga-Vieco AV, Esteban-Martinez L, Sanchez-Diaz M, Diaz-Garcia E, Santiago DJ, Rubio-Ponce A, Li JL, Balachander A, Quintana JA *et al* (2020) A Network of Macrophages Supports Mitochondrial Homeostasis in the Heart. *Cell* 183: 94-109 e123

Oh DS, Oh JE, Jung HE, Lee HK (2017) Transient Depletion of CD169(+) Cells Contributes to Impaired Early Protection and Effector CD8(+) T Cell Recruitment against Mucosal Respiratory Syncytial Virus Infection. *Front Immunol* 8: 819

Panizzi P, Swirski FK, Fig ueiredo JL, Waterman P, Sosnovik DE, Aikawa E, Libby P, Pittet M, Weissleder R, Nahrendorf M (2010) Impaired infarct healing in atherosclerotic mice with Ly-6C(hi) monocytosis. *J Am Coll Cardiol* 55: 1629-1638

Parmar T, Parmar VM, Perusek L, Georges A, Takahashi M, Crabb JW, Maeda A (2018) Lipocalin 2 Plays an Important Role in Regulating Inflammation in Retinal Degeneration. *J Immunol* 200: 3128-3141

Peng H, Long F, Ding C (2005) Feature selection based on mutual information: criteria of max-dependency, max-relevance, and min-redundancy. *IEEE Trans Pattern Anal Mach Intell* 27: 1226-1238

Percin GI, Eitler J, Kranz A, Fu J, Pollard JW, Naumann R, Waskow C (2018) CSF1R regulates the dendritic cell pool size in adult mice via embryo-derived tissue-resident macrophages. *Nat Commun* 9: 5279

Revelo X, Parthiban P, Chen C, Barrow F, Fredrickson G, Wang H, Yucel D, Herman A, van Berlo JH (2021) Cardiac Resident Macrophages Prevent Fibrosis and Stimulate Angiogenesis. *Circ Res*

Rojo R, Raper A, Ozdemir DD, Lefevre L, Grabert K, Wollscheid-Lengeling E, Bradford B, Caruso M, Gazova I, Sanchez A *et al* (2019) Deletion of a Csf1r enhancer selectively impacts CSF1R expression and development of tissue macrophage populations. *Nat Commun* 10: 3215

Ruedl C, Jung S (2018) DTR-mediated conditional cell ablation-Progress and challenges. *Eur J Immunol* 48: 1114-1119

Sager HB, Hulsmans M, Lavine KJ, Moreira MB, Heidt T, Courties G, Sun Y, Iwamoto Y, Tricot B, Khan OF *et al* (2016) Proliferation and Recruitment Contribute to Myocardial Macrophage Expansion in Chronic Heart Failure. *Circ Res* 119: 853-864

Schulz C, Gomez Perdiguero E, Chorro L, Szabo-Rogers H, Cagnard N, Kierdorf K, Prinz M, Wu B, Jacobsen SE, Pollard JW *et al* (2012) A lineage of myeloid cells independent of Myb and hematopoietic stem cells. *Science* 336: 86-90

Sivakumaran S, Henderson S, Ward S, Sousa PS, Manzo T, Zhang L, Conlan T, Means TK, D'Aveni M, Hermine O *et al* (2016) Depletion of CD11c(+) cells in the CD11c.DTR model drives expansion of unique CD64(+) Ly6C(+) monocytes that are poised to release TNF-alpha. *Eur J Immunol* 46: 192-203

Srinivas S, Watanabe T, Lin CS, William CM, Tanabe Y, Jessell TM, Costantini F (2001) Cre reporter strains produced by targeted insertion of EYFP and ECFP into the ROSA26 locus. *BMC Dev Biol* 1: 4

Stremmel C, Schuchert R, Schneider V, Weinberger T, Thaler R, Messerer D, Helmer S, Geissmann F, Frampton J, Massberg S *et al* (2018) Inducible disruption of the c-myb gene allows allogeneic bone marrow transplantation without irradiation. *J Immunol Methods* 457: 66-72

Stuart T, Satija R (2019) Integrative single-cell analysis. *Nat Rev Genet* 20: 257-272

Talbot J, Bianchini FJ, Nascimento DC, Oliveira RD, Souto FO, Pinto LG, Peres RS, Silva JR, Almeida SC, Louzada-Junior P *et al* (2015) CCR2 Expression in Neutrophils Plays a Critical Role in Their Migration Into the Joints in Rheumatoid Arthritis. *Arthritis Rheumatol* 67: 1751-1759

Todica A, Beetz NL, Gunther L, Zacherl MJ, Grabmaier U, Huber B, Bartenstein P, Brunner S, Lehner S (2018) Monitoring of Cardiac Remodeling in a Mouse Model of Pressure-Overload Left Ventricular Hypertrophy with [(18)F]FDG MicroPET. *Mol Imaging Biol* 20: 268-274

Todica A, Zacherl MJ, Wang H, Boning G, Jansen NL, Wangler C, Bartenstein P, Kreissl MC, Hacker M, Brunner S *et al* (2014) In-vivo monitoring of erythropoietin treatment after myocardial infarction in mice with [(6)(8)Ga]Annexin A5 and [(1)(8)F]FDG PET. *J Nucl Cardiol* 21: 1191-1199

Weinberger T, Esfandyari D, Messerer D, Percin G, Schleifer C, Thaler R, Liu L, Stremmel C, Schneider V, Vagnozzi RJ *et al* (2020) Ontogeny of arterial macrophages defines their functions in homeostasis and inflammation. *Nat Commun* 11: 4549

Weinberger T, Schulz C (2015) Myocardial infarction: a critical role of macrophages in cardiac remodeling. *Front Physiol* 6: 107

Xu P, Zhang J, Wang H, Wang G, Wang CY, Zhang J (2017) CCR2 dependent neutrophil activation and mobilization rely on TLR4-p38 axis during liver ischemia-reperfusion injury. *Am J Transl Res* 9: 2878-2890

Yates AD, Achuthan P, Akanni W, Allen J, Allen J, Alvarez-Jarreta J, Amode MR, Armean IM, Azov AG, Bennett R *et al* (2020) Ensembl 2020. *Nucleic Acids Res* 48: D682-D688

Zaman R, Epelman S (2022) Resident cardiac macrophages: Heterogeneity and function in health and disease. *Immunity* 55: 1549-1563

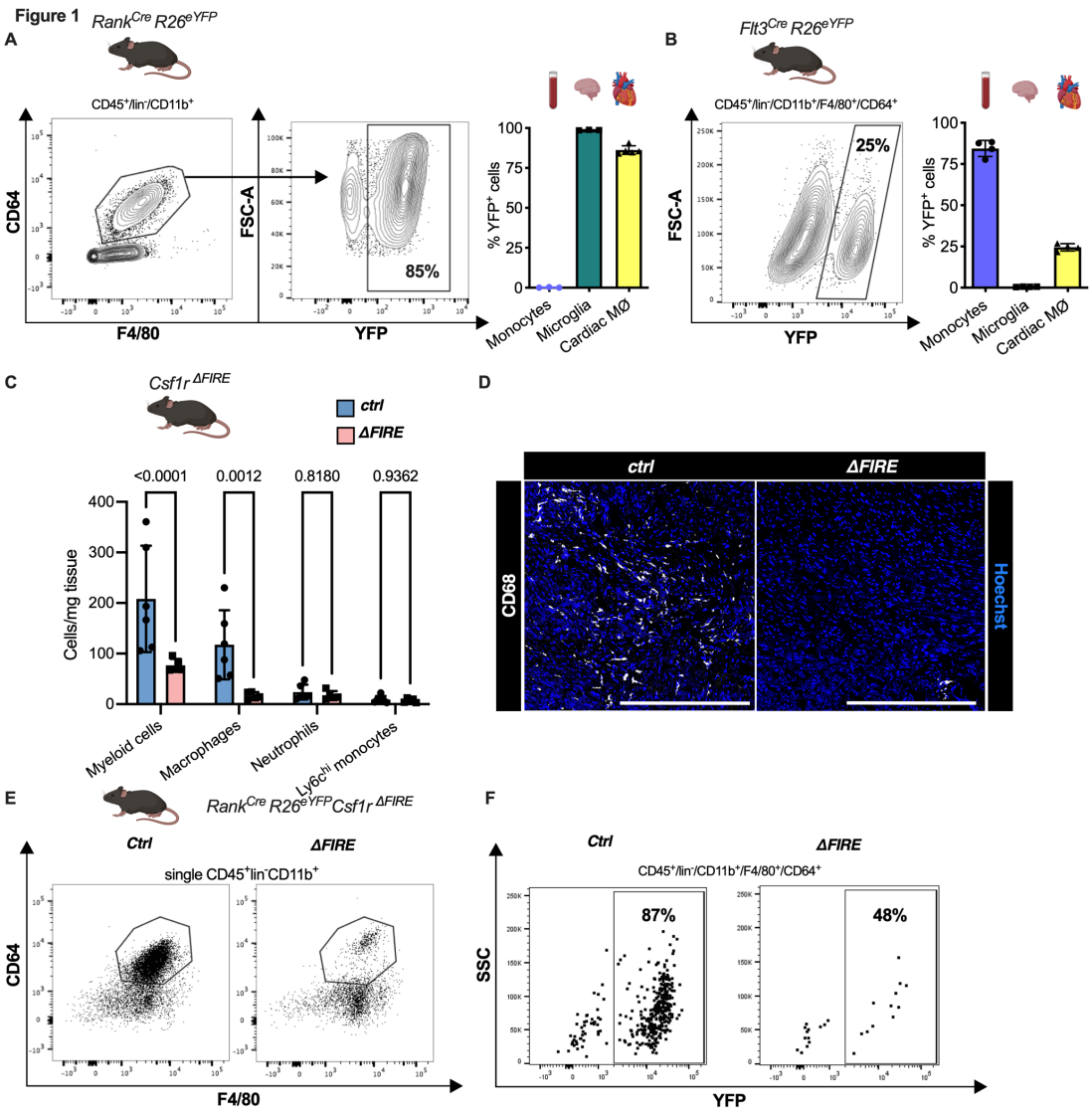

Figure 1. Absence of resident cardiac macrophages in *Csf1r*$^{\Delta FIRE}$ mice.
(A) Flow cytometry analysis of 3 month-old *Rank*^{Cre}*Rosa26*^{eYFP} mice, showing single/CD45$^+$/lin$^-$ (CD11c, Ter119, Tcrß, Nk1.1)/CD11b$^+$ cardiac cells, eYFP expression in macrophages (CD64$^+$/F4/80$^+$) and percentage of eYFP$^+$ blood monocytes, microglia and cardiac macrophages (n=3-5 each from an independent experiment). (B) Flow cytometry analysis of 3 month-old *Flt3*^{Cre}*Rosa26*^{eYFP} mice, showing macrophage expression of eYFP and percentage of eYFP$^+$ blood monocytes, microglia and cardiac macrophages (n=4 each from an independent experiment). **(C)** Number of myeloid cells (CD45$^+$/lin$^-$/CD11b$^+$), macrophages (CD45$^+$/lin$^-$/CD11b$^+$/CD64$^+$/F4/80$^+$), neutrophils (CD45$^+$/lin$^-$/CD11b$^+$/CD64$^-$/F4/80$^-$/Ly6g$^+$) and Ly6c^{hi} monocytes (CD45$^+$/lin$^-$/CD11b$^+$/CD64$^-$/F4/80$^-$/Ly6g-/Ly6c^{hi}) (*n=6 for control* and n=5 for Δ*FIRE* mice, each single experiments). **(D)** Representative immunohistological images showing macrophages (CD68$^+$ cells in white and Hoechst in blue) in *control* and Δ*FIRE* hearts in 3 month-old mice at baseline conditions (scale bars represent 500µm). **(E)** Representative flow cytometry analysis of cardiac macrophages and **(F)** their expression of eYFP in *Csf1r*$^{\Delta FIRE/+}$*Rank*^{Cre}*Rosa26*^{eYFP} *and Csf1r*$^{\Delta FIRE/\Delta FIRE}$*Rank*^{Cre}*Rosa26*^{eYFP}. Either Fisher's LSD test or unpaired t-test were performed and mean ± SD is shown.

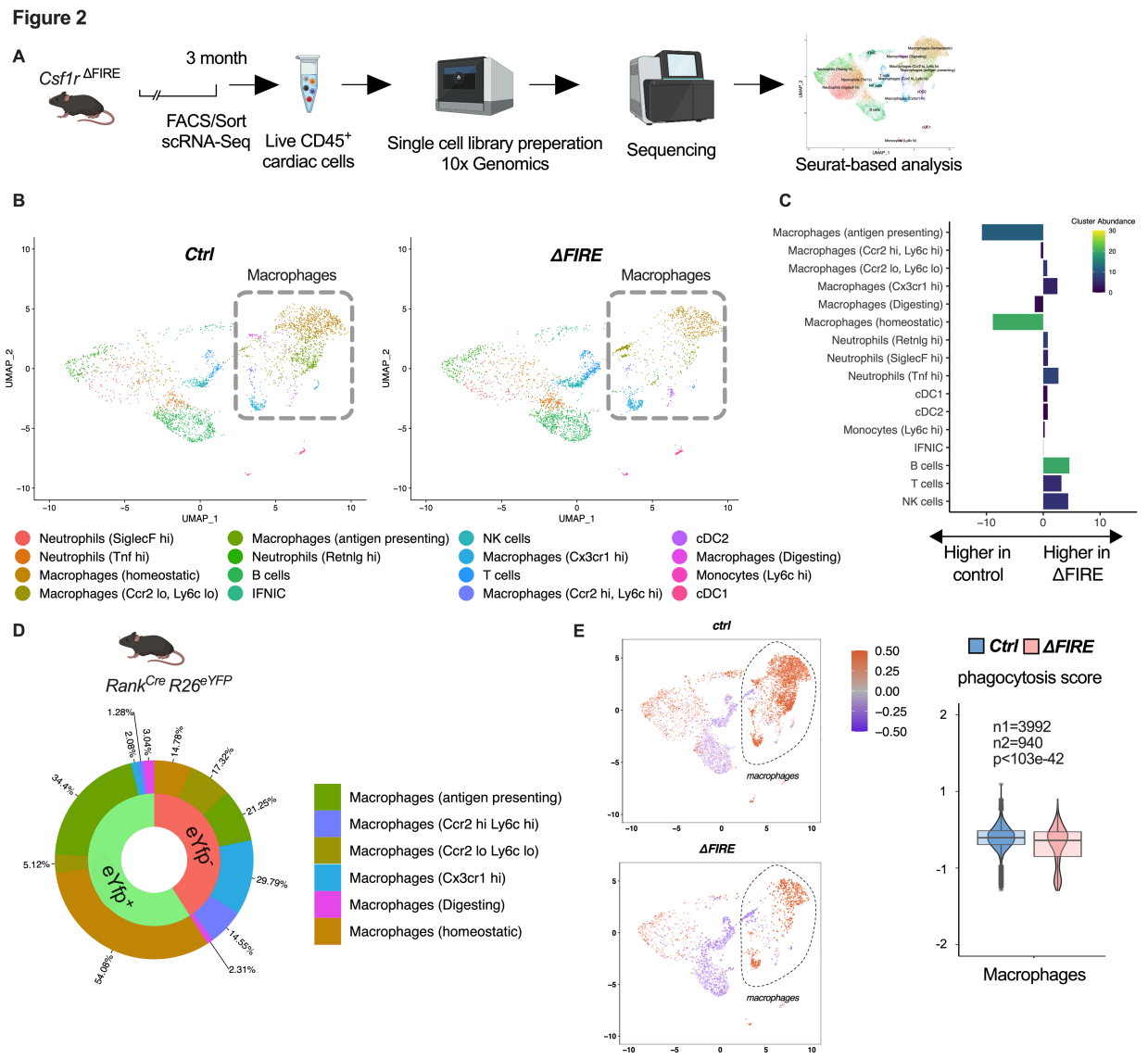

Figure 2. Changes in the cardiac immune phenotype in *Csf1r*$^{\Delta FIRE}$ mice in baseline conditions. **(A)** Experimental setup to analyze cardiac immune cells using scRNA-seq of sorted CD45^{+}/live cells. **(B)** UMAPs of control and ΔFIRE in baseline conditions (n=3 for *control* and Δ*FIRE)* **(C)** Absolute difference (percentage points) in cluster abundance between *control* and Δ*FIRE*. **(D)** Contribution of EMP-derived (*eYfp* expressing) macrophages to the different macrophage clusters analysed by scRNA-seq analysis of immune cells harvested from a *Rank*^{Cre}*Rosa26*^{eYFP} mouse. **(E)** Phagocytosis score projected on a UMAP displaying *control and* Δ*FIRE* immune cell subsets. Violin and box plots show the computed phagocytosis score combined in all macrophage clusters (n1/n2 represents number of cells from control/ Δ*FIRE* mice).

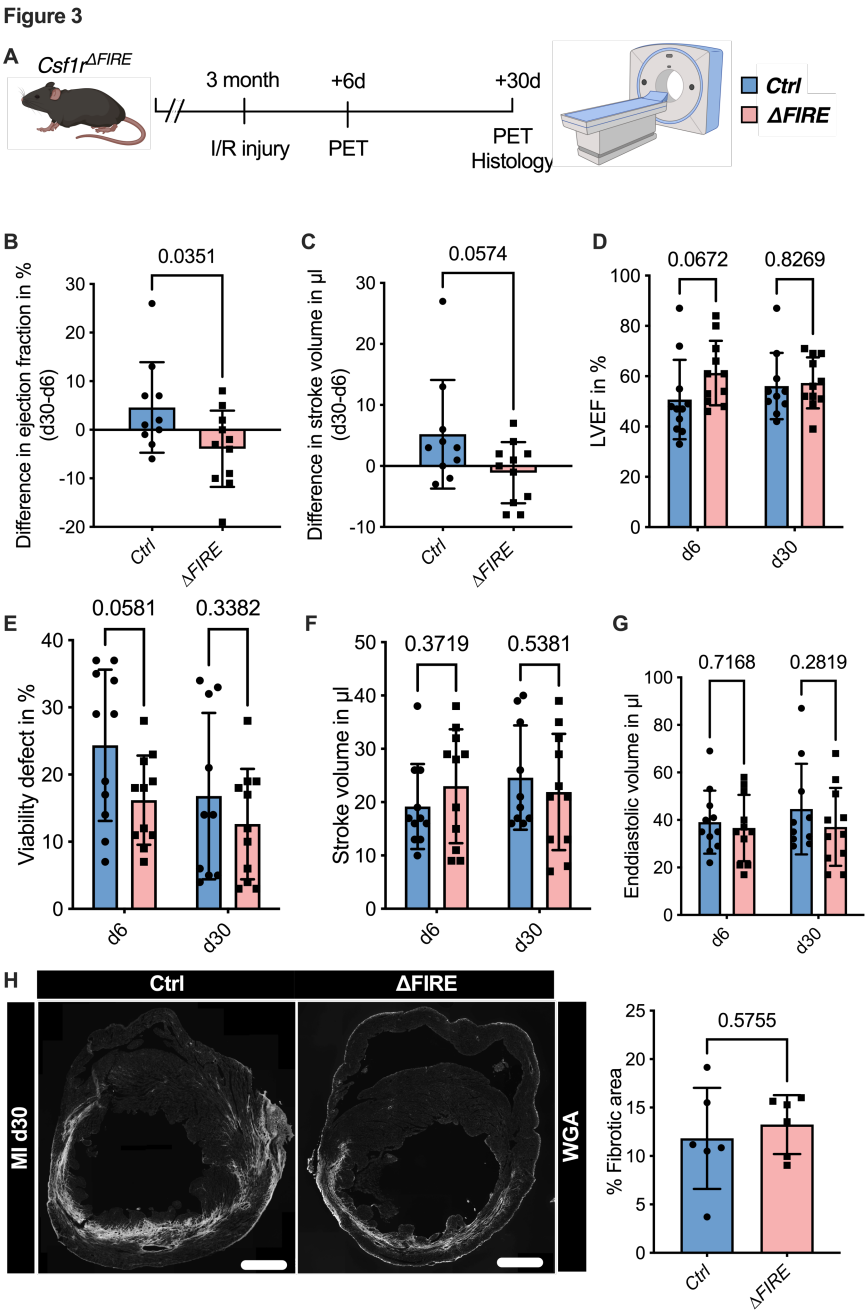

Figure 3. Adverse cardiac remodeling in *Csf1r*$^{\Delta FIRE}$ mice after I/R injury

(A) Schematic of the sequential analysis of cardiac function, dimensions and viability using positron-emission tomography 6 and 30 days after I/R injury in *control* and Δ*FIRE* with (B and C) showing the intraindividual changes in each parameter from d6 to d30 and (D-G) the individual timepoints on d6 and d30 (d6: n=11 for *control and* Δ*FIRE*, d30: n=10 for *control and n=11 for* Δ*FIRE*). **(B and D)** left ventricular ejection fraction (LVEF), **(C and E)** percentage of the viability defect, **(F)** stroke volume and **(F)** left-ventricular end-diastolic volume**.** **(H)** Representative immunohistological images showing the fibrotic area (WGA^{+} area) in hearts from *control and ΔFIRE* mice 30 days after I/R injury. Right panel shows the percentage of fibrotic area in the respective groups (n= 6 for each group). Student's t-test was performed and mean ± SD is shown.

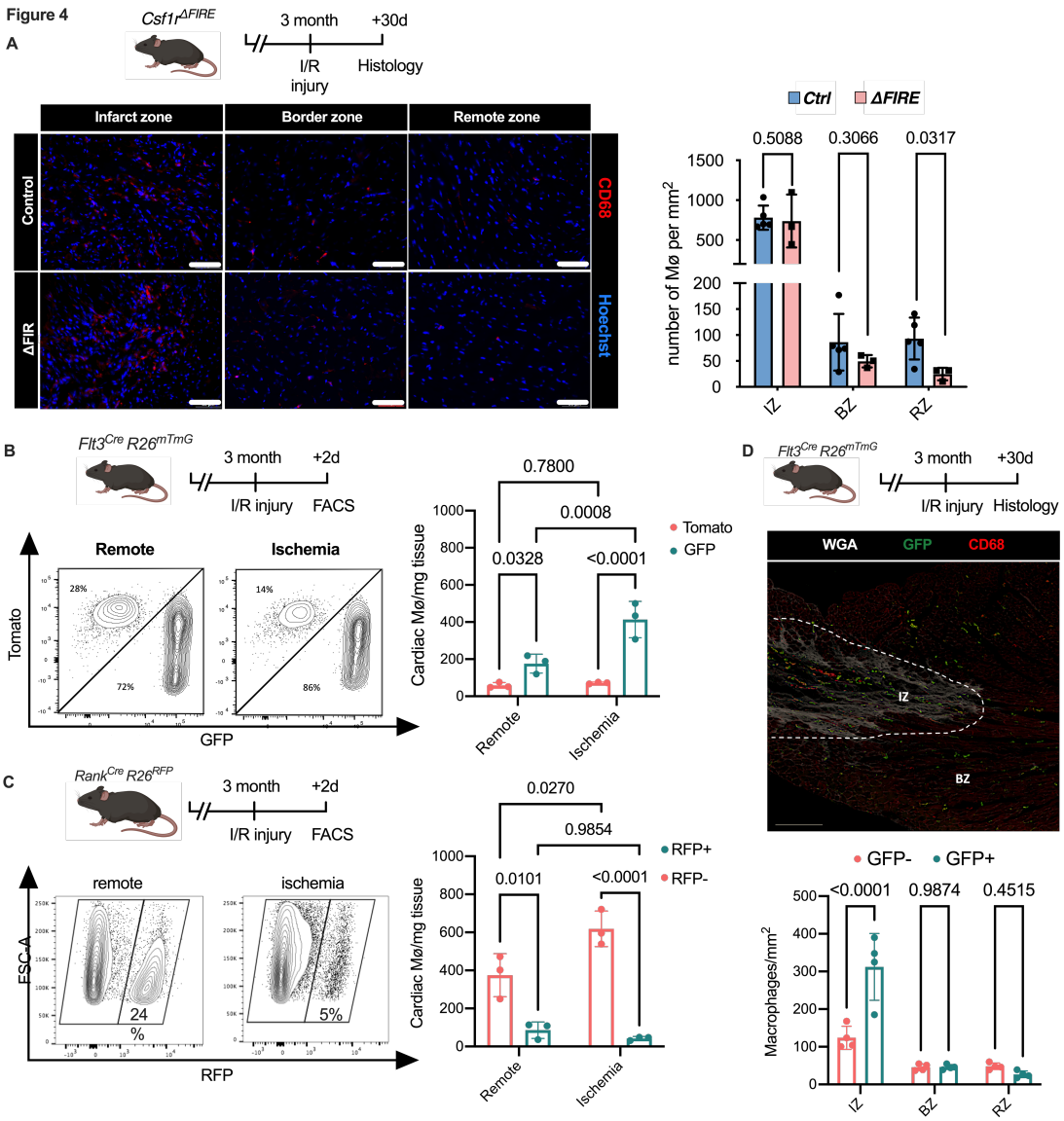

Figure 4. Recruitment of BM-derived macrophages into infarct zone of *Csf1r*$^{\Delta FIRE}$ mice.
(A) Representative immunohistology of hearts from Δ*FIRE* mice 30 days after I/R injury showing macrophages (CD68^{+} cells in red and Hoechst in blue) in the infarct, border and remote zone. Right panel shows number of cardiac macrophages in the respective area (n=5 *control* and n=3 for Δ*FIRE*). **(B)** Flow cytometry analysis of *Flt3*^{Cre}*Rosa26*$^{mT/mG}$ mice 2 days after I/R injury, (left) representative flow cytometry showing expression of tomato and GFP in macrophages in the remote and ischemic myocardium and (right) number of tomato^{+} and GFP^{+} cardiac macrophages in the respective area (n=3, each individual experiments). **(C)** Flow cytometry analysis of *Rank*^{Cre}*Rosa26*^{RFP} mice 2 days after I/R injury, (left) representative flow cytometry showing expression of RFP in macrophages in the remote and ischemic myocardium and (right) number of RFP^{-} and RFP^{+} cardiac macrophages in the respective area (n=3, each individual experiments). **(D)** Histological analysis of *Flt3*^{Cre}*Rosa26*$^{mT/mG}$ mice 30 days after I/R injury in the infarct, border and remote zone, (left) representative immunohistology of the infarct and border zone and (right) number of GFP^{-} and GFP^{+} cardiac macrophages in the respective areas (n=4). Fishers LSD test was performed for all experiments and mean ± SD is shown.

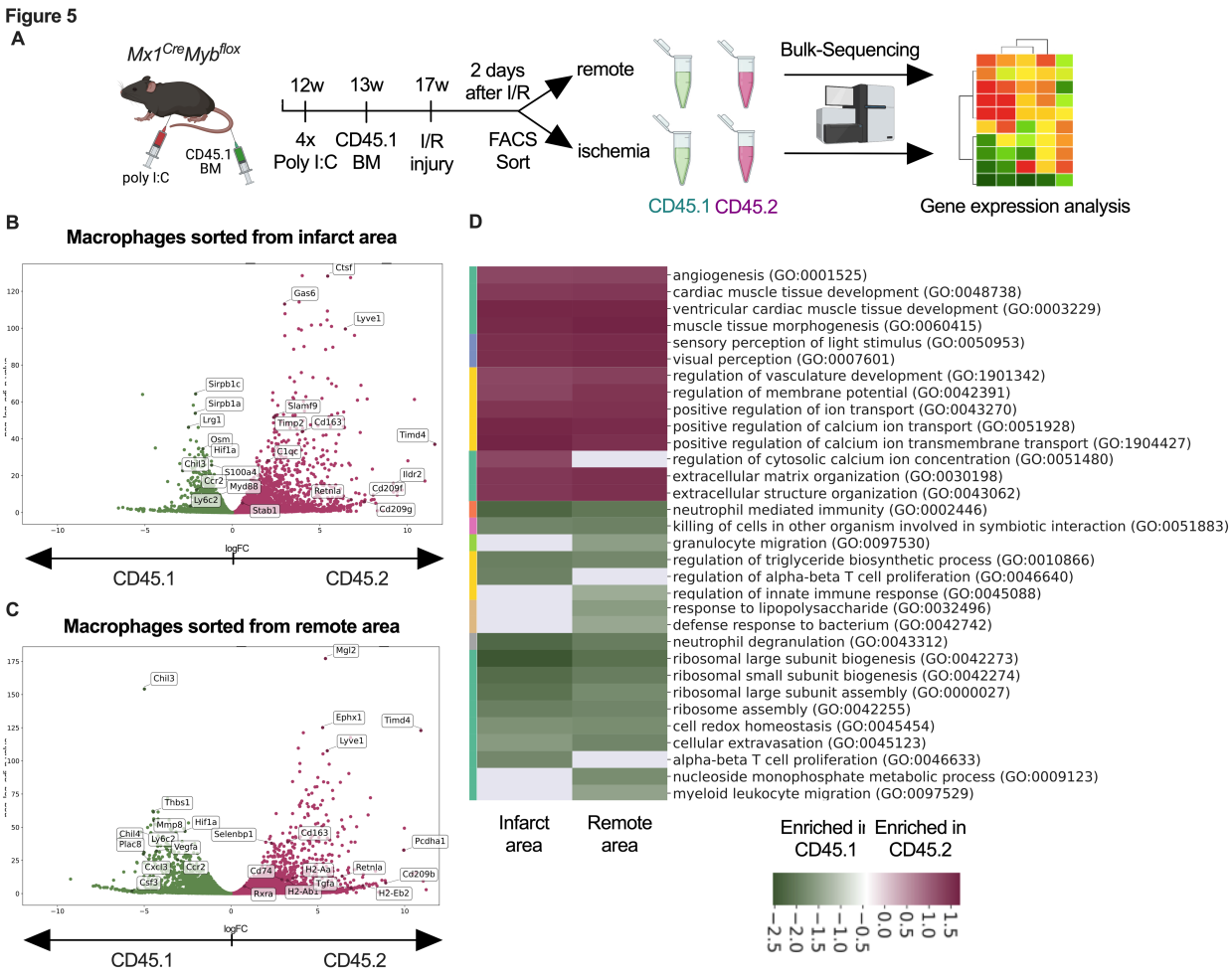

Figure 5. Transcriptional landscape of resident versus recruited macrophages in I/R injury

(A) Experimental setup to generate non-irradiation BM chimera using *CD45.2 Mx1*^{Cre}*Myb*$^{flox/flox}$ and transplantation of CD45.1 BM. I/R injury was induced 4 weeks after BM-transplantation and CD45.1^{+} and CD45.2^{+} macrophages were sorted from the remote and ischemic myocardium 2 days after I/R injury and RNA-sequencing was performed on bulk cells**. (B and C)** Volcano plot showing differential gene expression analysis results of recruited CD45.1 vs. resident CD45.2 macrophages in the **(B)** remote and **(C)** ischemic zone. **(D)** Gene ontology enrichment analysis showing specific biological processes enriched in CD45.1 and CD45.2 macrophages in the ischemic and remote zone.

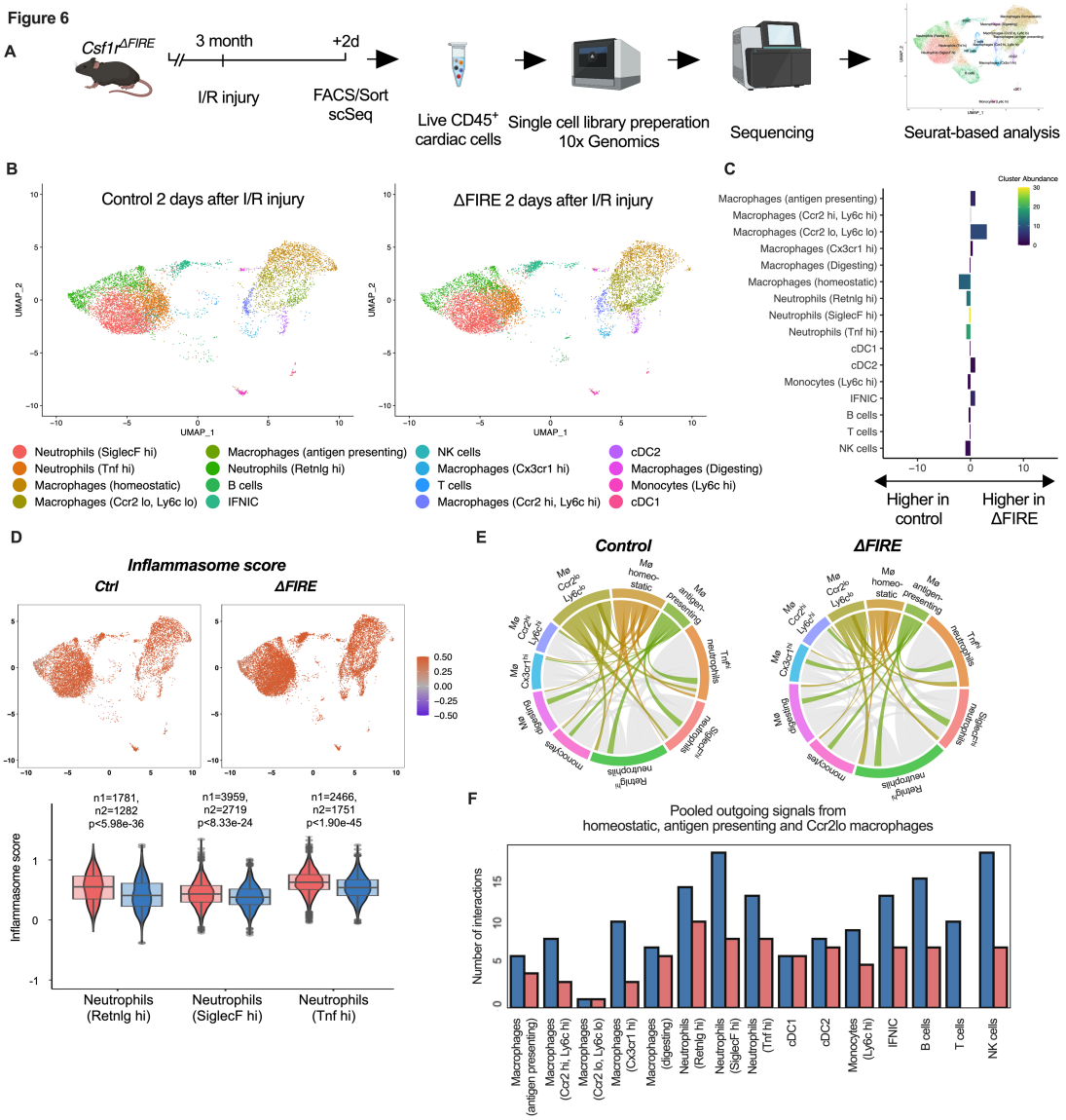

Figure 6. **Altered inflammatory patterns and immune cell communication in *Csf1r*$^{\Delta FIRE}$ mice.** **(A)** Experimental setup to analyze transcriptional changes in cardiac immune cells on a single cell level 2 days after I/R injury in *ΔFIRE* mice. **(B)** UMAPs of control and ΔFIRE 2 days after I/R injury (n=2 for *control* and Δ*FIRE)*. **(C)** Absolute difference (percentage points) in cluster abundance between *control* and Δ*FIRE*. **(D)** Inflammasome score projected on a UMAP displaying control and ΔFIRE immune cell subsets after I/R injury. Violin and box plots show the computed inflammasome score in neutrophil clusters (n1/n2 represents number of cells from control/ Δ*FIRE* mice). (**E**) Ligand–receptor interactions of *antigen-presenting, Ccr2*^{lo} *ly6c*^{lo} *and homeostatic macrophages* (highlighted) with other immune cell clusters. Shown are the aggregated communication scores (width of interactions) for all cell types. Only communication scores larger than 6 are considered. (**F**) Number of interactions (with communication score > 6) outgoing from homeostatic, antigen presenting and Ccr2^{lo} macrophages to other immune cell clusters.

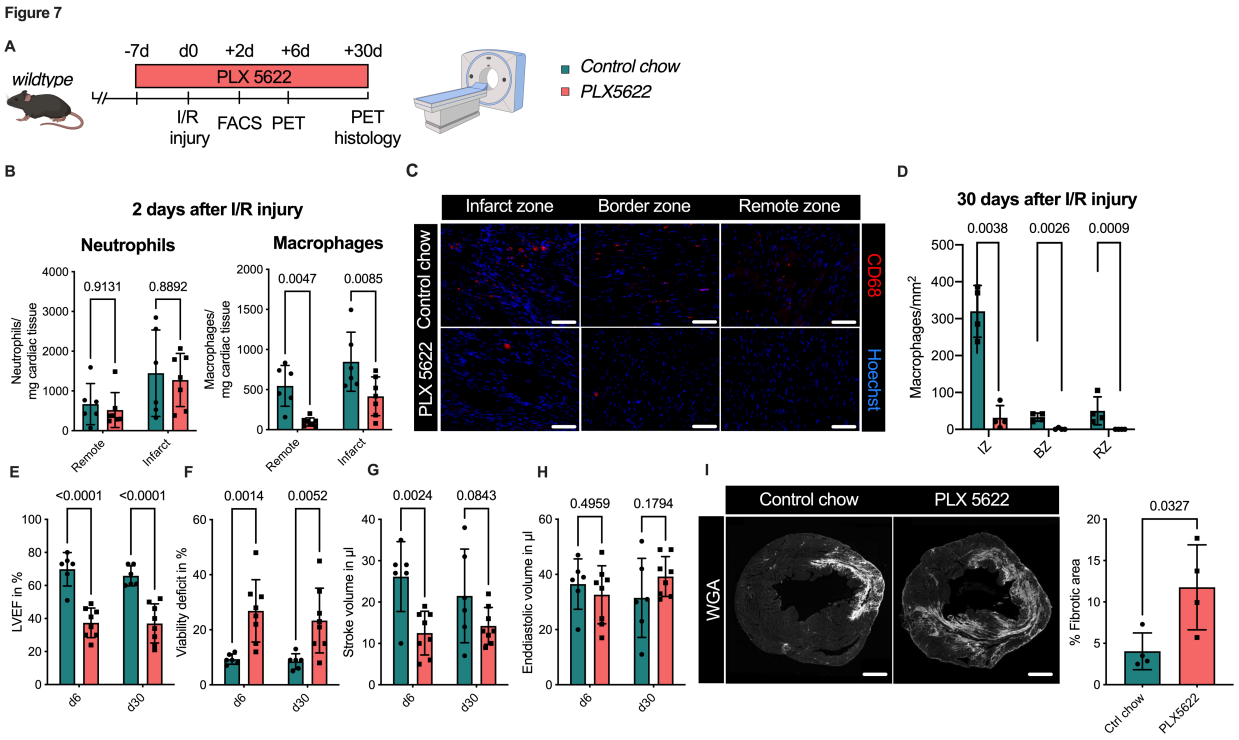

Figure 7. Ablation of resident and recruited macrophages severely impacts on cardiac healing after I/R injury

(A) Schematic of the analysis of cardiac function and infarct size in mice treated with PLX5622 7 days prior and 30 days after I/R injury. **(B)** Number of cardiac macrophages and neutrophils in the remote and ischemic myocardium 2 days after I/R injury in mice fed control chow (n=6) or PLX5622 (n=7). **(C)** Representative immunohistology of hearts 30 days after I/R injury showing macrophages ($CD68^+$ cells in red and Hoechst in blue) in the infarct, border and remote zone and **(D)** number of cardiac macrophages in the respective area (n=4 for control chow and n=4 for PLX5622). **(E)** Left ventricular ejection fraction (LVEF), **(F)** viability deficit, **(G)** stroke volume and **(H)** end-diastolic volume measured using positron-emission tomography 6 and 30 days after I/R injury (n=6 for control chow, n=8 for PLX5622). **(I)** Representative immunohistological images showing the fibrotic area (WGA^+ area) in hearts 30 days after I/R injury from mice fed control chow or PLX5622. Percentage of fibrotic area in the respective groups (n= 4 for each group). Student's t-test or Fishers LSD test was performed and mean ± SD is shown.